ACS APPLIED MATERIALS & INTERFACES

Research Article

www.acsami.org

Ultrasensitive and Selective Detection of Dopamine Using Cobalt-Phthalocyanine Nanopillar-Based Surface Acoustic Wave Sensor

Najla Fourati,*[,†] Mahamadou Seydou,[‡] Chouki Zerrouki,[†] Ajay Singh,[§] Soumen Samanta,[§] François Maurel,[‡] Dinesh K. Aswal,[§] and Mohamed Chehimi[‡,∥]

[†]CNRS-ENS Cachan-Cnam, SATIE, UMR 8029 , 292 rue Saint Martin, 75003 Paris, France

[‡]Sorbonne Paris Cité, ITODYS, UMR 7086, CNRS, Université Paris Diderot, 15 rue J-A de Baïf, 75013 Paris, France

[§]Technical Physics Division, Bhabha Atomic Research Center, Mumbai 400 085, India

[∥]CNRS UMR 7182 ICMPE, Université Paris-Est Créteil, 2-8 rue Henri Dunant, 94320 Thiais, France

ABSTRACT: A highly selective and sensitive surface acoustic wave (SAW) sensor of dopamine (DA) was developed by depositing cobalt phthalocyanine (CoPc) nanopillars on gold-coated sensing platform of SAW sensor. The developed biosensor presents a sensitivity of 1.6°/nM, has a low limit of detection (LOD) on the order of 0.1 nM, and imparts more selectivity toward DA, since the detection limit of the interfering ascorbic acid (AA) is as high as 1 mM. To understand the selectivity mechanisms of this sensor toward DA, density functional theory-based chemical calculations were carried out. Calculations suggest two different types of interactions: dative bond with a very strong character for DA-CoPc complexes, and significant ionic character in the case of AA-CoPc ones. The interaction energies, in liquid phase, were estimated to be equal to −81 kJ mol^{-1} and −38 kJ mol^{-1} for DA-CoPc and AA-CoPc complexes, respectively, therefore accounting for the selective detection of DA over AA using tandem CoPc nanopillar-based SAW sensor device. This work demonstrates a simple and efficient design of SAW sensors employing thin nanostructured CoPc biomolecular recognition layers for DA detection.

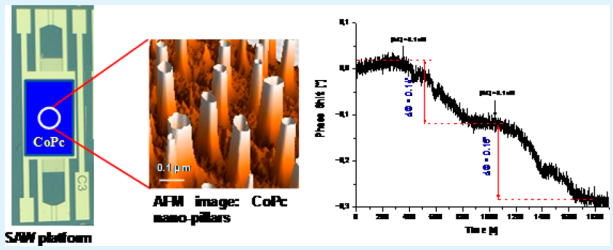

KEYWORDS: *SAW sensor, cobalt phthalocyanine, dopamine, ascorbic acid, chemical calculations*

1. INTRODUCTION

Dopamine (DA) is an important neurotransmitter in mammalian central nervous systems, and the loss of DA-containing neurons may result in serious diseases such as schizophrenia and Parkinson's diseases.[1−3] However, there exist some challenges to measuring DA under physiological conditions. The main ones are related to the coexistence of very low levels of DA with high levels of ascorbic acid (AA) in organisms. In fact, AA is not only present in the brain, but it also releases during neuronal activity and by some psychoactive drugs.[4] In the case of DA detection by commonly employed electrochemical methods, limitations are related to the fact that DA oxidized at almost the same potential as AA. Nevertheless, recent publications have highlighted several strategies to overcome this problem using new nanocomposites,[5−10] magnetic particles,[11−16] conducting polymer,[17,18] carbon nanotubes,[19−25] and molecularly imprinted polymers as active layers.[26−30] However, the development of these electrochemical sensors requires yet large numbers of steps for fabrication. As alternatives to electrochemical methods, one can design gravimetric sensors such as quartz crystal microbalance (QCM) and surface acoustic wave (SAW) sensors.[31,32] These methods could also be combined with electrochemistry for the fabrication of sensing layers.[33,34] To the best of our knowledge not much work has been done to detect dopamine using SAW sensors. The basic principle of SAW sensors is the detection of changes in the propagation characteristics of the surface acoustic waves, which are caused by perturbations on the active surface of the device. The physical, chemical, or biological variations, occurring on the sensor sensitive area, can be estimated from the output signal by measuring insertion loss, phase shift, or oscillation frequency. Since frequency (or phase) can be measured with extremely high precision, test molecules/gas/liquids can often be detected at extremely low concentrations.[34−43] Still, one must design efficient sensing layers for the target analytes, and the approach might be simple or tedious. In the present work, we functionalized the SAW sensor by metal phthalocyanine (MPcs) thin films, as sensing layer. MPc thin layers have been widely used as recognition layers in gas sensors.[44−49] In the present work we demonstrate that cobalt phthalocyanine (CoPc) thin films, grown by molecular beam epitaxy on sensing platform of SAW sensors, can act as extremely selective and sensitive layers for the detection of DA. To the best of our knowledge this is first ever report on MPc-based SAW sensor to detect a neurotransmitter in liquid media with lowest detection limit of 0.1 nM. The

Received: September 17, 2014
Accepted: November 20, 2014
Published: November 20, 2014

experimental results of CoPc-based SAW sensor was supported by theoretical results obtained by chemical calculation based on the density functional theory (DFT).

2. EXPERIMENTAL SECTION

2.1. Chemicals. Dopamine (DA), cobalt phthalocyanine (CoPc), ascorbic acid (AA), phosphate-buffered saline (PBS) BioReagent pH 7.4 for molecular biology, H_2SO_4 (95%), and H_2O_2 (30%) were procured from Sigma-Aldrich. DA and AA were used as received.

2.2. Details of SAW Sensor Fabrication. The developed sensor consists of dual delay lines fabricated on a 36° YX-$LiTaO_3$ piezoelectric substrate. Sensitive area as well as the interdigital transducers (IDTs) were realized by evaporation of (20/80) nm Cr/Au layers. The IDTs were photolithographically patterned with a periodicity of $\lambda = 40$ μm, which corresponds to an operating frequency of ~104 MHz (Figure 1a). Each electrode consists of 30 double finger

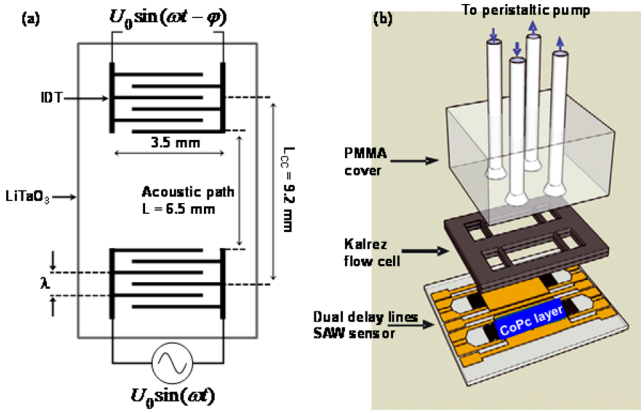

Figure 1. Schematic representation of (a) $LiTaO_3$ surface acoustic wave sensor. (b) Parts of the measurement setup for use in liquid media.

pairs, minimizing thus triple transit interferences. The measurement setup consists of a CoPc-coated SAW sensor, a Kalrez flow cell deposited on the sensing region, to which is associated a poly(methyl methacrylate) cover including inlets and outlets (Figure 1b) connected to a peristaltic pump, and an HP8711C network analyzer. Before depositing CoPc films, SAW devices were immersed for 30 min into a piranha solution (1:1 (v/v) 98% H_2SO_4/30% H_2O_2), then rinsed with ultrapure water three times and immediately dipped in a methanol solution. This procedure is followed to obtain a clean and preactivated surface, suitable for deposition of CoPc films. Finally the SAW devices were dried using N_2 gas and immediately loaded into the molecular beam epitaxy vacuum chamber (base vacuum $\approx 2 \times 10^{-8}$ mbar) for deposition of 50 nm thick CoPc films. The growth temperature and deposition rate were, respectively, 50 °C and 2 Å·s^{-1}. After that, CoPc-coated SAW devices were taken out of vacuum chamber for further characterization.

2.3. AFM Measurements. Atomic force microscopy measurements were carried out with a Nanosurf easyScan 2 Flex system in the dynamic force mode, with cantilever's resonance frequency of about 165 kHz. Commercially available tips (ACLA silicon AFM probes from AppNANO) with curvature radius ~6 nm were used. The different scans were performed under ambient conditions.

3. CALCULATION METHODS

Chemical calculations were performed based on DFT. The minimum structures and the electronic and free energies corresponding to the isolated and complex stable conformers, were calculated at the B3LYP/6-311+G* level of theory.[50] The tight termination criteria (Berny algorithm) optimization procedure as implemented in Gaussian09 was used. The geometries were fully optimized at the B3LYP/GEN level by using 6-311+G(d) basis set for H, C, N, O atoms and LANL2DZ basis set for Co atom in the gas phase. The analyses of vibrational frequencies indicated that optimized structures of complexes were at stationary points corresponding to local minima without imaginary frequencies. The basis set superposition error is not corrected here, so interaction energies are overstated. Solvent (water) effect is taken into account by polarisable continuum model[51] (PCM) with Kohn–Sham united atomic topologies cavities (UAKS) as implemented in Gaussian09.[52] Free energies of complex in solution were derived by means of thermodynamic cycle applied to systems in gas phase with correction for solvation energies. Stabilization or formation energies $\Delta E_s = E_{A-B} - (E_A + E_B)$ were calculated as the difference between the energy of relaxed complex E_{A-B} and the sum of energies of isolated systems relaxed separately. In our case, E_{A-B} is the energy of complex CoPc and DA or AA, E_A is the energy of AA or DA, and E_B is the energy of CoPc. As we compare here energy differences between complexes, the basis set superposition error was not corrected.

4. RESULTS AND DISCUSSION

4.1. Morphology and Structure of CoPc Films Grown on Sensing Platform of SAW Sensor. A typical AFM image of a gold sensing area of the SAW sensor reveals a granular morphology with average grain size on the order of 100 nm (Figure 2a). These grains are protruding out, as revealed by the

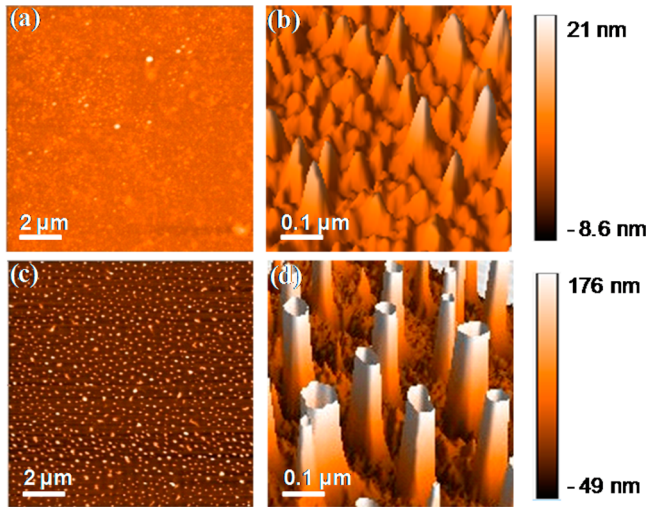

Figure 2. AFM images of (a) 2D scan of gold sensing area of the SAW sensor, (b) the corresponding 3D high-magnification image, (c) 2D scan of 50 nm thick CoPc film grown over the gold sensing platform of the SAW sensor, (d) 3D view of the high-magnification image of CoPc films.

three-dimensional (3D) high-magnification image (Figure 2b). The two-dimensional (2D) AFM image of a 50 nm thick CoPc film, grown over the SAW sensing area, shows that a CoPc layer grows up as quasi-regularly spaced spherical grains with an average size of ~100 nm (Figure 2c). The 3D magnified view reveals that quasi-periodically spaced spherical grains are protruding out of the substrate plane like nanopillars whose heights vary between 60 and 130 nm, whereas spacing varies between 300 and 650 nm (Figure 2d). The surface roughness of these CoPc films was found to be equal to 32.7 nm (in the spatial frequency range: 2×10^{-2} to 20.5 μm^{-1}). Notice that

dx.doi.org/10.1021/am506403f | ACS Appl. Mater. Interfaces 2014, 6, 22378–22386

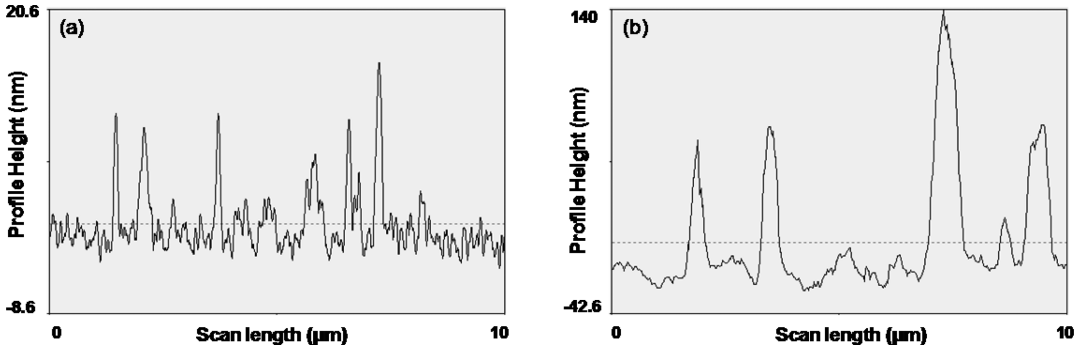

Figure 3. Cross section of AFM images sensing area of the SAW sensor (a) bare gold (b) after the deposition of 50 nm thick CoPc film.

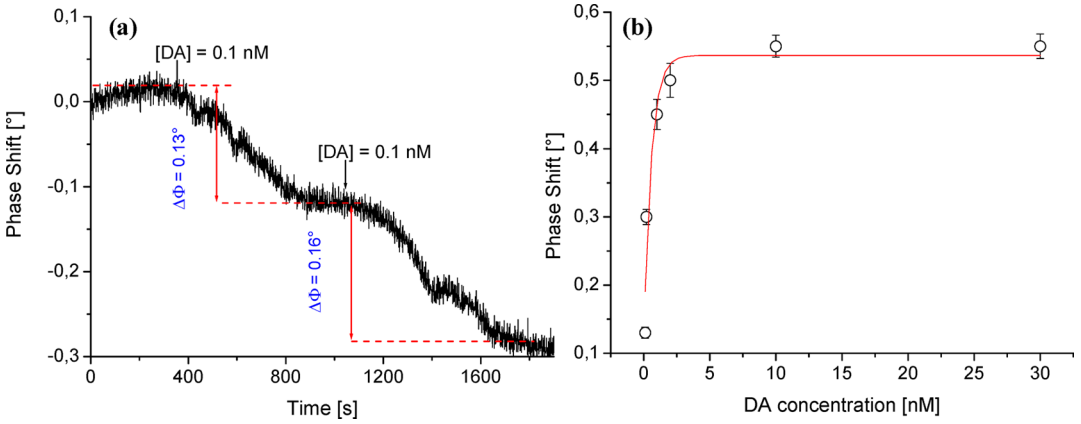

Figure 4. (a) Phase variations vs time after two successive injections of 0.1 nM of a DA solution. (b) Phase shifts as a function of DA concentration.

such nanopillar morphology with an extended surface area may be highly suitable for sensing applications.

Now we discuss the origin of such well-separated nanopillar morphology of the CoPc films over the gold-coated sensing platform of the SAW sensor. The growth mechanisms of organic films on inorganic substrates are complicated phenomena because of the noncovalent interactions at the interface, which are molecule−molecule and molecule−substrate. These two interactions allow molecules to adsorb on the substrate surface in edge-on or face-on configurations. Moreover, as the properties of thin films are very sensitive to the substrate nature, layers of a same material and a same thickness may present different physical/morphological properties when the substrate is modified. Most studies agree on the fact that the first growth process leads to the appearance of isolated islets, on the substrate surface, which rise independently to a critical thickness, beyond which the islands coalesce and the thin film becomes continuous. This thickness depends on the nature of the material and the substrate, the speed of deposition, and the temperature, and it varies typically from 10 to 20 nm.[53,54] For the particular case of metallic phthalocyanine, previous studies[55,56] have shown that up to a critical thickness (until which molecule−substrate interaction dominates over molecule−molecule interaction), metallic phthalocyanine thin film growth initially takes place via face-on configuration over the gold surface (and edge-on configuration at higher thicknesses). The reported value of critical thickness for CoPc over gold surface is ∼10 nm. On the basis of these reports, it can be speculated that initially CoPc grows up in face-on configuration on the nanospherical grains of gold, and then grain growth is more favorable perpendicular to the substrate plane. Notice that even if the used high-vacuum evaporation can contribute to this particular growth, we think that the key factor is rather the substrate surface. Indeed, in previous works using high-vacuum evaporation of CoPc on flexible polymeric substrate, no comparable structures were observed by AFM.[57]

In Figure 3, we represented a cross section of AFM images of the SAW sensing area before and after the deposition of a 50 nm thick CoPc film. Higher and less numerous peaks appear in the case of a CoPc film cross-section (Figure 3b) compared to that of a bare gold surface (Figure 3a). To highlight the previous idea, we considered two other statistical parameters to characterize the previous images of Figure 2: the maximum surface peak height S_p and the maximum surface valley depth S_v. For the bare gold surface, we founded S_p = 41 nm and S_v = −6 nm. That means that the bare surface consists mainly of peaks, which constitute a favorable condition for CoPc growth perpendicular to the substrate plane. After the deposition of a CoPc film, S_p and S_v were found equal to 474 nm and −45 nm, respectively. The substrate surface features were thus reproduced and amplified. This is also in line with our assumption that the dominant peaks were the seat of the first molecule−substrate interaction.

4.2. Sensor Performance Evaluation. The sensing area of the CoPc SAW sensor was first rinsed with a PBS solution, and then DA solution was injected. The typical response curve (i.e., phase shift vs time) after the injection of two successive concentrations [0.1 nM] of DA is shown in Figure 4a. It appears that, within uncertainties, phase-shift values are comparable after exposures to the same DA concentration. The repeatability of the developed sensor is on the order of

14%. From Figure 4a it can also be seen that these sensors exhibit a response time of ∼500 s, a value that is in the same order of magnitude as other SAW sensor applications [35]. Sensitivity of the developed sensor, calculated from the slope of the phase/concentration curve, was found equal to 1.6°/nM. This value is sufficiently high to foreshadow further easy detection of DA with concentrations in the subnanomolar range. The lowest detection limit (LDL) of ∼0.1 nM is significantly lower than 26 nM characteristic of living systems,[58] making thus disease diagnosis, using the present SAW sensor, possible in further developments.

Phase-shift variations ($\Delta\Phi$) versus DA concentration (C), plotted in Figure 4b, can be fitted with the "One-site binding" equation: $\Delta\Phi = (B \times C)/(K + C)$, where $B = 0.558 \pm 0.018$ [deg] is the maximum sensor's response to the specific binding (CoPc-DA), reached when all the interaction sites are blocked (due to full coverage of the sensing layer); and $K = 0.227 \pm 0.038$ [nM] represents the equilibrium binding constant.

4.3. Selectivity Test. Useful biosensors must be selective in addition to being sensitive. To investigate selectivity, the developed SAW sensor was exposed to ascorbic acid solutions. From Figure 5, it can be seen that, for concentrations of AA in the range of $[10^{-6} - 10^{-4}]$ M, no noticeable changes in the phase shift were recorded. The sensor starts giving response at an AA concentration of 10^{-3} M: a phase shift on the order of 0.19° is observed. The CoPc film–based SAW sensors are thus highly selective to DA in comparison to AA.

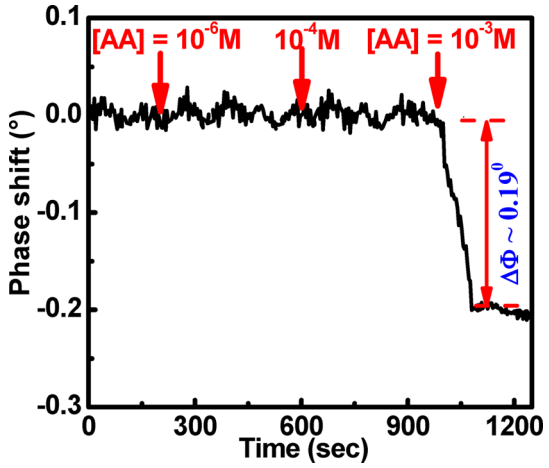

Figure 5. Response of the CoPc-based SAW sensor for different AA concentrations.

5. CHEMICAL CALCULATIONS

5.1. Isolated Systems Conformational Landscape. To explore the potential energy landscape of DA and AA, we applied an optimized scan with a pitch of 10°, from −180 to 180°, on the main dihedral angle, denoted θ, which defines the tail position relative to the ring (Figure. 6). The corresponding potential energy landscape, for both DA and AA, released at B3LYP/6-31G* is also presented in Figure. 6. The most stable conformers, corresponding to the minima of energy, were fully optimized with the large and diffuse basis set 6-311+G* and selected to complex with the template.

5.1.1. Dopamine. The systematic conformational search realized at B3LYP/6-31G* shows the existence of four minima. All of them were fully optimized at the improvement calculation level (B3LYP/6-311+G*). Results show that the increase in basis set size changes the relative conformational energies and reduces the conformational landscape from four to three stable conformers.

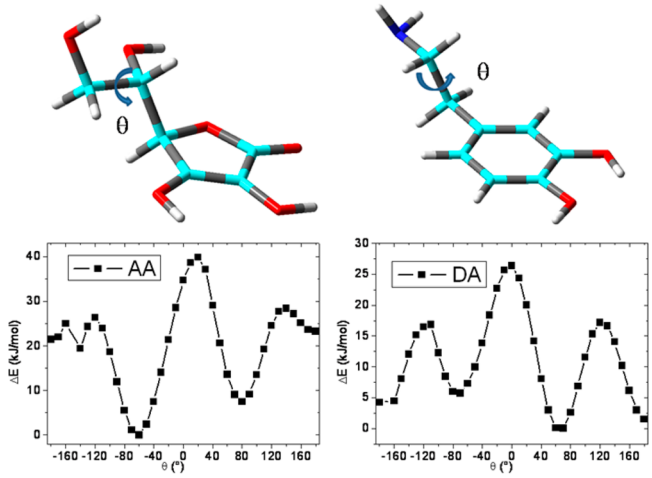

Figure 6. Structures and potential energy landscape of AA (left) and DA (right) in function of dihedral angle θ at the B3LYP/6-31G* level of calculation.

Using the large basis set 6-311+G*, the most stable conformer is DAI, with a final torsion angle of 60°. DAII and DAIII are less stable than DAI by 0.60 and 6.04 kJ mol^{-1}, respectively (Table 1). The optimized dihedral angle θ values are −178° and −72° for DAII and DAIII, respectively.

Recently, the conformational landscape of dopamine has been investigated by experimental rotational spectra and theoretical calculations through a systematic variation of the dihedral angles that determine the conformation of the side chains and OH group position of dopamine.[59] These previous results suggested the presence of seven conformers for the neurotransmitter; however, the most stable ones are those we found by means of B3LYP/6-311+G*level (see Table 1).

5.1.2. Ascorbic Acid. The L-ascorbic acid used in the experiment can adopt two tautomeric forms depending on protonated sites. A previous study showed that the most stable tautomer is that for which the two oxygen atoms in the β position relative to the oxygen atom of the ring are protonated.[60]

According to the flexible tail, different conformers could be present. Results, presented in Figure 6, show the existence of four stable conformers (which were optimized with a large basis set 6-311+G*) and that the most stable one (AAI) has a final torsion angle of −62°. AAII, AAIII, and AAIV are less stable than AAI by 2.26, 7.55, and 21.62 kJ mol^{-1}, respectively (Table 1). These results are in a good agreement with those of Yadav et al.[61]

5.1.3. Cobalt Phthalocyanine (CoPc). Calculations were done for different symmetries with LANL2DZ on Co and 6311+G* basis set on the over atoms. We found that the most stable configuration is planar with D_{4h} symmetry, in agreement with previous observations where it was shown that for the 3-fold symmetry of the Au (111) surface, the symmetry of the adsorbed planar metallophthalocyanine (MPc) molecules is reduced from D_{4h} to C_{2v}.[62]

5.2. Complex Formation. The conformers of both DA and AA were attached to CoPc by chemical intuition to establish metal nitrogen or oxygen ionic covalent bond and hydrogen

Table 1. Dihedral Angles, Relative Energies of Conformers Compared to the Lowest Energy Conformations of DA and AA Calculated at the B3LYP/6-311+G* Level

molecule	DA			AA			
conformer	III	I	II	II	I	III	IV
dihedral angle θ (deg)	−72	60	−178	180	−62	81	172
ΔE (kJ mol^{-1})	6.04	0.00	0.60	2.26	0.00	7.55	21.62

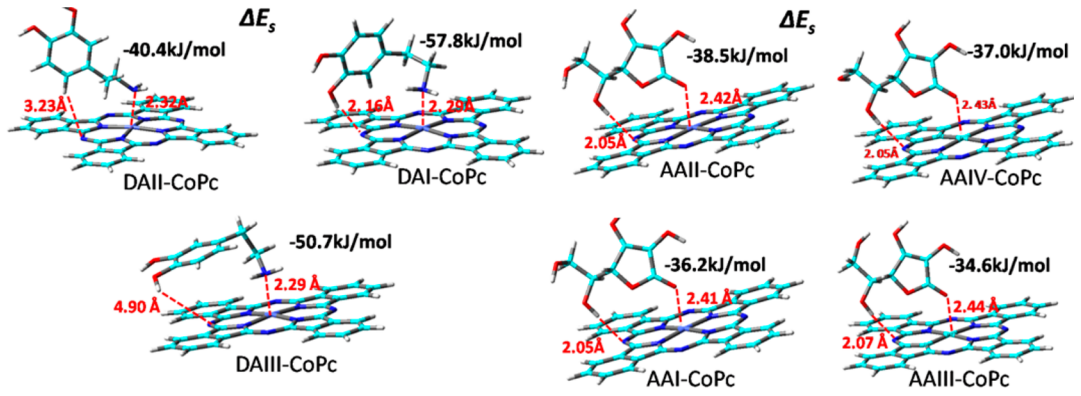

Figure 7. Structures of stable conformers of DA-CoPc and AA-CoPc complexes (the formation energies and geometrical parameters $d_{H\cdots N}$ and $d_{Co-N(O)}$ are inserted).

bond interactions. The complexes were fully optimized at B3LYP/6-311+G* level, and normal mode vibration frequencies were computed to ensure that they are really local minima. The results are reported in Figure 7.

The most stable configuration for dopamine corresponds to the case where nitrogen atoms are placed above cobalt atom to form Co−N dative bond. The Co···O interaction was also interrogated by placing oxygen atom above Co. The obtained complexes are not stable, and the geometry changes drastically. The most stable structure is that for which one strong hydrogen bond takes place between one OH group of dopamine and the nitrogen of phthalocyanine ($d_{H\cdots NPc}$ = 2.16 Å) in addition to the dative bond (Co−N = 2.29 Å) (Figure 6). In our case, the most stable complex is DAI-CoPc, for which the formation energy was found equal to −58 and −81 kJ mol^{-1} in gas and liquid phases, respectively. It is noteworthy that the Co−N dative length value is in a good agreement with the experimental and theoretical values obtained in refs 63 and 64.

The two other structures are less stable with formation energies of −51 and −40 kJ mol^{-1} in gas phase. In the DAIII-CoPc complex, dopamine conformer is linked essentially by Co−N dative bond in addition to a weak $\pi-\pi$ stacking. The comparison of DAI-CoPc and DAIII-CoPc complex leads to evaluate the Co−N bond formation energy. The dihedral angle values are not modified significantly by adsorption. They derived from isolated values of +11°, 0°, and −6° for DAIII, DAII, and DAI, respectively. Our results are in line with those of the previous work of Ponce et al.[65] who investigated, by both experimental and theoretical studies, the formation of self-assembly monolayers involving cobalt phthalocyanines anchored by 4-aminothiophenol and 4-mercaptopyridine to the Au (111) surface. They found dative bond lengths of 2.06 and 2.39 Å for 4-mercaptopyridine and 4-aminothiophenol, respectively.

In the case of AA, the most stable AA-Pc complex corresponds to that where a dative bond takes place between the oxygen of carbonyl group and cobalt atom. The complexes are stabilized also by one hydrogen bond between the OH group of the tail and one nitrogen atom of phthalocyanine as shown in Figure 7. The formation energies of these complexes are much closed and vary from −34 to −38 kJ mol^{-1}. Our values are, however, higher than those obtained by Sun et al.[66] for oxygen molecule adsorption on CoPc (−27.7 kJ mol^{-1}). This difference could account for the presence of hydrogen bond between AA and CoPc. By taking into account the solvation influence, the formation energy decreases to −60 kJ mol^{-1} for the AAII-CoPc conformation. As the energies of formation, the length of the dative bonds, and the hydrogen bonds vary slightly between conformations, the Co−O dative length varies from 2.41 to 2.44 Å, while the hydrogen bond length varies in the range of 2.05−2.07 Å. The dihedral angles of AA conformers are not significantly modified by the complex formation. They remain unchanged for all conformers except for AAII where a shift of 4° was recorded.

Comparing the two molecules of interest, we can observe that CoPc affinity is more important for DA than AA with more than 20 kJ mol^{-1} in both gas and aqueous phases. This result is in concordance with metal−ligand bond length. In the case of DA, the Co−N bond length (2.29 Å) matches the sum of covalent radii of N and Co (2.01 Å). For AA, the Co−O (2.40 Å) is larger than the sum of O and Co covalent radii (1.99 Å). These results argue for the formation of a dative bond between Co and N, while C and O are expected to develop a rather ionic bond. The hydrogen bonds lengths H···NCoPc for DA and AA complexes are 2.16 and 2.05 Å, respectively. The six-coordinate Co complexes were investigated by adding two molecules DA or AA around CoPc. Formation energies per molecule, in gas phase, were found equal to −48 and −33 kJ mol^{-1} for DA and AA complexes, respectively. It may be noted that in both cases the formation energy decreases proving that the pentacoordinate complex is more stable than the six-coordinate CoPc complexes. The lengths of dative CO−N(O) bonds increase from pentacoordinate values of ∼0.14 (0.10) Å, and hydrogen bond OH···NPc changes to 2.04 Å.

The Mulliken charges on cobalt, those of the nitrogen atom of dopamine and the oxygen atom of AA carbonyl group are gathered in Table 2. Results show an important charge transfer

Table 2. Formation Energies, Dative and Hydrogen Bond Lengths, and Mulliken Atomic Charges on Nitrogen (qN), Oxygen (qO), Cobalt(qCo), and Nitrogen of DAI, AAII, CoPc, DAI-CoPc, and AAII-CoPc

isolated or complex	ΔEs (kJ mol^{-1})	Co···N(O) (Å)	H···N (Å)	qN (O) (au)	qCo (au)	qNPc (au)
DAI				−0.63		
AAII				−0.33		
CoPc					0.98	0.06
DAI-CoPc	−57.8	2.29	2.16	−0.02	0.73	0.08−0.27
AAII-CoPc	−38.5	2.43	2.05	0.06	0.530	0.16−0.38

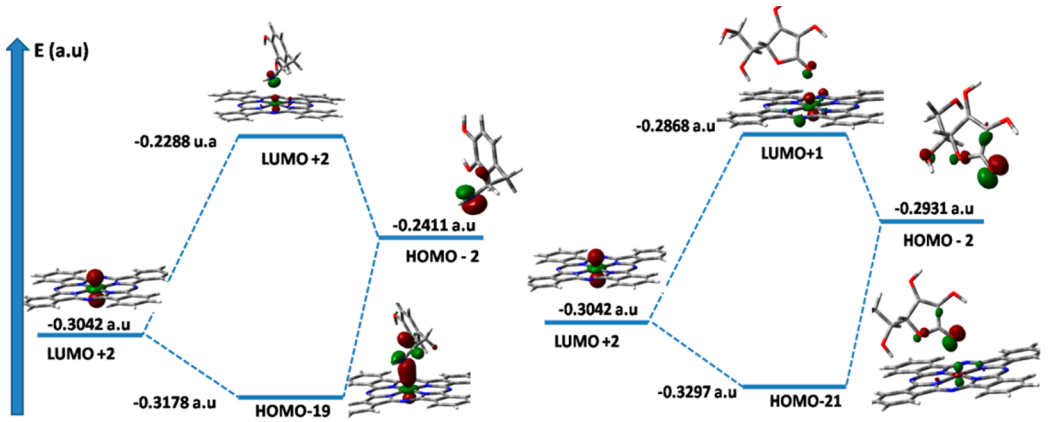

Figure 8. Frontier molecular orbital overlap between CoPc and DA and AA.

between cobalt atom and oxygen or nitrogen atom of AA and DA. This charge transfer is more important for AA (0.45 e$^-$) than it is for DA (0.25 e$^-$). This observation proves that the ionic character is more pronounced for Co−O in AAII-CoPc. Note that part of the cobalt charge was transferred to its neighboring nitrogen denoted NPc in Table 2.

Results of frontier molecular orbital analyses around the highest occupied orbital (HOMO) and the lowest unoccupied orbital (LUMO) are summarized in Figure 8. For DA, the occupied orbital HOMO−2 corresponds to π orbital essentially localized on nitrogen atom. For CoPc, the unoccupied LUMO +2 orbital corresponds to d_{z^2} of cobalt atom. For AA, the occupied HOMO−2 orbital represents the lone pair π orbital localized in oxygen atom. The difference of energy between theses frontier orbitals is low and may allow an overlap between them. In addition to hydrogen bonds and the ionic part, the interaction between AA or DA and CoPc is dominated by the overlap between the unoccupied LUMO+2 (d_{z^2}) of CoPc and the occupied HOMO−2 (π) orbitals of DA or AA. The products of this interaction are the bonding orbital HOMO−19 and the antibonding LUMO+2 in the DA complex and HOMO−21 and LUMO+1 for the AA one. Similar types of interaction were found in previous study carried out on NO molecule adsorption on CoPc.[67] In the case of AA, and because of hybridization, one can observe that the position of the lone pair orbital cannot allow maximizing the overlap with d_{z^2}. This could explain the low energy of formation. In contrast to AA, the occupied π orbital, located on N atom of DA, takes place perfectly above Co and gives better recovery with d_{z^2} of CoPc. This may explain why the dative bond is stronger for DA compared to AA.

6. SENSING MECHANISM

On the basis of the theoretical calculations results, we propose that the interaction between DA and CoPc is mediated by the formation of dative bond between N (from DA) and Co. In the formation of dative bond the lone pair of N gets transferred to $3d^7$ orbital of Co^{2+}. In case of AA and CoPc intercation is due to the formation of ionic bond between O (from AA) and Co. Further deep understanding of interaction can be understood by molecular orbital picture. For DA, the occupied orbital HOMO−2 corresponds to π orbital essentially localized on nitrogen atom. For CoPc, the unoccupied LUMO+2 orbital corresponds to d_{z^2} of cobalt atom. For AA, the occupied HOMO−2 orbital represents the lone pair π orbital localized in oxygen atom. The interaction between AA or DA and CoPc can be understood by the overlap between the unoccupied LUMO +2 (d_{z^2}) of CoPc and the occupied HOMO−2 (π) orbitals of DA or AA. In the case of AA, because of hybridization, one can observe that the position of the lone pair orbital cannot allow maximizing the overlap with d_{z^2} of CoPc. In contrast to AA, the occupied π orbital, located on N atom of DA, takes place perfectly above Co and gives better overlap with d_{z^2} of CoPc. This explains why CoPc SAW sensors respond to lower concentration of DA as compared to AA.

7. CONCLUSION

A SAW sensor coated with a thin layer of coablt(II) phthalocyanine has been developed for selective detection of dopamine. Results show that this device has an excellent dopamine sensing capability in the subnanomolar range, including a reasonably fast response, and low detection limit of 0.1 nM. The CoPc nanopillar-based SAW sensors were found to be highly selective toward dopamine in comparison to ascorbic acid. Chemical calculations, based on DFT, were performed to understand the high affinity of CoPc to dopamine in comparison to ascorbic acid. Results show the formation of a dative bond with a very strong character for dopamine-CoPc complex, while the analysis of Mulliken charges and frontier orbitals highlighted a significant ionic character in the case of ascorbic acid. The agreement between theoretical calculations and experimental results are not only encouraging but also pave

the way to more important developments of MPc-functionalized SAW sensors in applications where there is a demand for high sensitivity and extremely low limits of detection, associated with great selectivity.

AUTHOR INFORMATION

Corresponding Author

*E-mail: fourati@cnam.fr. Phone: +33 1 58 80 87 03.

Notes

The authors declare no competing financial interest.

ACKNOWLEDGMENTS

The authors would like to thank the Indo-French Centre for the Promotion of Advanced Research (IFCPAR) for financial supports through the "Flexi-Sensors" Project No. 4705-2. This work is also supported by "DAE-SRC Outstanding Research Investigator Award"(2008/21/05-BRNS) granted to D.K.A. This work was performed using HPC resources from GENCI-[CCRT/CINES/IDRIS] (Grant No. 2014-[c2014097006]).

REFERENCES

(1) Seeman, E.; Niznik, H. B. Dopamine Receptors and Transporters in Parkinson's Disease and Schizophrenia. *FASEB J.* **1990**, *4*, 2737−2744.

(2) Volkow, N. D.; Gur, R. C.; Wang, G. J.; Fowler, J. S.; Moberg, P. J.; Ding, Y. S.; Hitzemann, R.; Smith, G.; Logan, J. Association Between Decline in Brain Dopamine Activity With Age and Cognitive and Motor Impairment in Healthy Individuals. *Am. J. Psychiatry.* **1998**, *155*, 344−349.

(3) Winterera, G.; Weinberger, D. R. Genes, Dopamine and Cortical Signal-to-Noise Ratio in Schizophrenia. *Trends Neurosci.* **2004**, *27*, 683−690.

(4) Hadjiconstantinou, M. N.; Neff, H. Ascorbic Acid could be hazardous to your Experiments: a commentary on Dopamine Receptor Binding Studies with Speculation on a Role for Ascorbic Acid in Neuronal Function. *Neuropharmacology* **1983**, *22*, 939−943.

(5) Pandiselvi, K.; Thambidurai, S. Chitosan-ZnO/Polyanilne Nanocomposite Modified Glassy Carbon Electrode for Selective Detection of Dopamine. *Int. J. Biol. Macromol.* **2014**, *67*, 270−278.

(6) Ezhil Vilian, A. T.; Rajkumar, M.; Chen, S.-M. In Situ Electrochemical Synthesis of Highly Loaded Zirconium Nanoparticles Decorated Reduced Graphene Oxide for the Selective Determination of Dopamine and Paracetamol in Presence of Ascorbic Acid. *Colloids Surf., B* **2014**, *115*, 295−301.

(7) Lv, M.; Mei, T.; Zhang, C.; Wang, X. Selective and Sensitive Electrochemical Detection of Dopamine Based on Water-soluble Porphyrin Functionalized Graphene Nanocomposites. *RSC Adv.* **2014**, *4*, 9261−9270.

(8) Massoumi, B.; Fathalipour, S.; Massoudi, A.; Hassanzadeh, M.; Entezami, A. A. Ag/Polyaniline Nanocomposites: Synthesize, Characterization, and Application to the Detection of Dopamine and Tyrosine. *J. Appl. Polym. Sci.* **2013**, *130*, 2780−2789.

(9) Li, J.; Yang, J.; Yang, Z.; Li, Y.; Yu, S.; Xu, Q.; Hu, X. Graphene-Au Nanoparticles Nanocomposite Film for Selective Electrochemical Determination of Dopamine. *Anal. Methods* **2012**, *4*, 1725−1728.

(10) Liu, M.; Wang, L.; Deng, J.; Chen, Q.; Li, Y.; Zhang, Y.; Li, H.; Yao, S. Highly Sensitive and Selective Dopamine Biosensor Based on a Phenylethynyl Ferrocene/Graphene Nanocomposite Modified Electrode. *Analyst.* **2012**, *137*, 4577−4583.

(11) Ballesteros, C. A. S.; Cancino, J.; Marangoni, V.-S.; Zucolotto, V. Nanostructured Fe_3O_4 Satellite Gold Nanoparticles to Improve Biomolecular Detection. *Sens. Actuators, B* **2014**, *198*, 377−383.

(12) Herrasti, Z.; Martinez, F.; Baldrich, E. Electrochemical Detection of Dopamine Using Streptavidin-Coated Magnetic Particles and Carbon Nanotube Wiring. *Sens. Actuators, B* **2014**, *203*, 891−898.

(13) Teymourian, H.; Salimi, A.; Khezrian, S. Fe_3O_4 Magnetic Nanoparticles/Reduced Graphene Oxide Nanosheets as a Novel Electrochemical and Bioeletrochemical Sensing Platform. *Biosens. Bioelectron.* **2013**, *49*, 1−8.

(14) Wang, Z.; Bai, Y.; Wei, W.; Xia, N.; Du, Yi. Magnetic Fe_3O_4-based Sandwich-type Biosensor Using Modified Gold Nanoparticles as Colorimetric Probes for the Detection of Dopamine. *Materials* **2013**, *6*, 5690−5699.

(15) Lai, G.; Liu, Y.; Yu, A.; Han, D.; Zhang, H. Simultaneous Sensitive Determination of Dopamine and Uric Acid in the Presence of Excess Ascorbic Acid with a Magnetic Chitosan Microsphere/Thionine Modified Electrode. *Anal. Lett.* **2013**, *46*, 1525−1536.

(16) Chandra, S.; Arora, K.; Bahadur, D. Impedimetric Biosensor Based on Magnetic Nanoparticles for Electrochemical Detection of Dopamine. *Mater. Sci. Eng., B* **2012**, *177*, 1531−1537.

(17) Weaver, C. L.; Li, H.; Luo, X.; Cui, X. T. A Graphene Oxide/Conducting Polymer Nanocomposite for Electrochemical Dopamine Detection: Origin of Improved Sensitivity and Specificity. *J. Mater. Chem. B* **2014**, *2*, 5209−5219.

(18) Sasso, L.; Heiskanen, A.; Diazzi, F.; Dimaki, M.; Castillo-León, J.; Vergani, M.; Landini, E.; Raiteri, R.; Ferrari, G.; Carminati, M.; Sampietro, M.; Svendsen, W.-E.; Emnéus, J. Doped Overoxidized Polypyrrole Microelectrodes as Sensors for the Detection of Dopamine Released from Cell Populations. *Analyst* **2013**, *138*, 3651−3659.

(19) Yu, B.; Yuan, H.; Yang, Y.-Y.; Cong, H.-L.; Hao, T.-Z.; Xu, X.-D.; Zhang, X.-L.; Yang, S.-J.; Zhang, L.-X. Detection of Dopamine using Self-Assembled Diazoresin/Single-Walled Carbon Nanotube Modified Electrodes. *Chin. Chem. Lett.* **2014**, *25*, 523−528.

(20) Manjunatha, J. G.; Deraman, M.; Basri, N.-H.; Nor, N.-S.; Talib, I.-A.; Ataollahi, N. Sodium Dodecyl Sulfate Modified Carbon Nanotubes Paste Electrode as a Novel Sensor for the Simultaneous Determination of Dopamine, Ascorbic Acid, and Uric Acid. *C. R. Chim.* **2014**, *17*, 465−476.

(21) Cesarino, I.; Galesco, H.-V.; Moraes, F.-C.; Lanza, M-R-V.; Machado, S. Biosensor Based on Electrocodeposition of Carbon Nanotubes/Polypyrrole/Laccase for Neurotransmitter Detection. *Electroanalysis* **2013**, *25*, 394−400.

(22) Bujduveanu, M.-R.; Yao, W.; Le Goff, A.; Gorgy, K.; Shan, D.; Diao, G.-W.; Ungureanu, E.-M.; Cosnier, S. Multiwalled Carbon Nanotube-$CaCO_3$ Nanoparticle Composites for the Construction of a Tyrosinase-Based Amperometric Dopamine Biosensor. *Electroanalysis* **2013**, *25*, 613−619.

(23) Zheng, S.; Huang, Y.; Cai, J.; Guo, Y. Nano-Copper-MWCNT-Modified Glassy Carbon Electrode for Selective Detection of Dopamine. *Int. J. Electrochem. Sci.* **2013**, *8*, 12296−12307.

(24) Jyothirmayee Aravind, S. S.; Ramaprabhu, S. Dopamine Biosensor with Metal Oxide Nanoparticles Decorated Multi-Walled Carbon Nanotubes. *Nanosci. Methods* **2012**, *1*, 102−114.

(25) Adekunle, A.-S.; Farah, A.-M.; Pillay, J.; Ozoemena, K.-I.; Mamba, B.-B.; Agboola, B.-O. Electrocatalytic Properties of Prussian Blue Nanoparticles Supported on Poly(m-aminobenzenesulphonic acid)-Functionalised Single-Walled Carbon Nanotubes towards the Detection of Dopamine. *Colloids. Surf., B* **2012**, *95*, 186−194.

(26) Do, P.-T.; Do, P.-Q.; Nguyen, H.-B.; Nguyen, V.-C.; Tran, D.-L.; Le, T.-H.; Nguyen, L.-H.; Pham, H.-V.; Nguyen, T.-L.; Tran, Q.-H. A Highly Sensitive Electrode Modified with Graphene, Gold Nanoparticles, and Molecularly Imprinted Over-Oxidized Polypyrrole for Electrochemical Determination of Dopamine. *J. Mol. Liq.* **2014**, DOI: 10.1016/j.molliq.2014.07.029.

(27) Lei, Y.; Xu, G.; Wei, F.; Yang, J.; Hu, Q. Preparation of a Stir Bar Coated with Molecularly Imprinted Polymer and its Application in Analysis of Dopamine in Urine. *J. Pharm. Biomed. Anal.* **2014**, *94*, 118−124.

(28) Bali Prasad, B.; Jauhari, D.; Prasad Tiwari, M. A Dual-Template Imprinted Polymer-Modified Carbon Ceramic Electrode for Ultra Trace Simultaneous Analysis of Ascorbic Acid and Dopamine. *Biosens. Bioelectron.* **2013**, *50*, 19−27.

(29) Gam-Derouich, S.; Jouini, M.; Ben Hassen-Chehimi, D.; Chehimi, M. M. Aryl Diazonium Salt Surface Chemistry and Graft Photopolymerization for the Preparation of Molecularly Imprinted Polymer Biomimetic Sensor Layers. *Electrochim. Acta* **2012**, *73*, 45−52.
(30) Chen, P. Y.; Nien, P. C.; Ho, K. C. Highly Selective Dopamine Sensor Based on an Imprinted SAM/Mediator Gold Electrode. *Procedia Chem.* **2009**, *1*, 285−288.
(31) Zhou, W.-H.; Tang, S.-F.; Yao, Q.-H.; Chen, F.-R.; Yang, H.-H.; Wang, X.-R. A Quartz Crystal Microbalance Sensor Based on Mussel-Inspired Molecularly Imprinted Polymer. *Biosens. Bioelectron.* **2010**, *26*, 585−589.
(32) Wang, J.-L.; Ren, K.-F.; Chang, H.; Zhang, S.; Jin, L.-J.; Ji, J. Facile Fabrication of Robust Superhydrophobic Multilayered Film Based on Bioinspired Poly(dopamine)-Modified Carbon Nanotubes. *Phys. Chem. Chem. Phys.* **2014**, *16*, 2936−2943.
(33) Lattach, Y.; Fourati, N.; Zerrouki, C.; Fougnion, J. M.; Garnier, F.; Remita, S. Surface Acoustic Wave Sensor Combining Gravimetric and Electrochemical Transductions: Application for Atrazine Detection. *Sens. Lett.* **2011**, *9*, 2249−2252.
(34) Lattach, Y.; Fourati, N.; Zerrouki, C.; Fougnion, J. M.; Garnier, F.; Prenelle, C.; Remita, S. Molecularly Imprinted Surface Acoustic Wave Sensors: The Synergy of Electrochemical and Gravimetric Transductions in Chemical Recognition Processes. *Electrochim. Acta* **2012**, *73*, 36−44.
(35) Zerrouki, C.; Fourati, N.; Lucas, R.; Vergnaud, J.; Fougnion, J. M.; Zerrouki, R.; Pernelle, C. Biological Investigation using Shear Horizontal Surface Acoustic Wave Sensor: Small "Click Generated" DNA Hybridization Detection. *Biosens. Bioelectron.* **2010**, *26*, 1759−1762.
(36) Luo, J.; Luo, P.; Xie, M.; Du, K.; Zhao, B.; Pan, F.; Fan, P.; Zeng, F.; Zhang, D.; Zheng, Z.; Liang, G. A New Type of Glucose Biosensor Based on Surface Acoustic Wave Resonator using Mn-Doped ZnO Multilayer Structure. *Biosens. Bioelectron.* **2013**, *49*, 512−518.
(37) Luo, J.; Xie, M.; Luo, P.; Zhao, B.; Du, K.; Fan, P. A Sensitive Glucose Biosensor without using Glucose Test Strips Based on ZnO/SiO_2/Si Surface Acoustic Wave Device. *Mater. Lett.* **2014**, *130*, p14−16.
(38) Gruhl, F.-J.; Länge, K. Surface Modification of an Acoustic Biosensor Allowing the Detection of low Concentrations of Cancer Markers. *Anal. Biochem.* **2012**, *420*, 188−190.
(39) Otori, H.; Higashiyama, T.; Uehara, A.; Kainuma, M.; Kudo, Y.; Kamimura, T.; Kon, T.; Mochitate, K.; Kikuchi, H.; Furuya, Y. Signal Change of Surface Acoustic Wave (SAW) caused by H_2O_2 Damage to SV40-T2 Cells Cultivated on SH-SAW Sensor. *Sens. Actuators, B* **2013**, *200*, 162−167.
(40) Bröker, P.; Lücke, K.; Perpeet, M.; Gronewold, T-M-A. A Nanostructured SAW Chip-Based Biosensor Detecting Cancer Cells. *Sens. Actuators, B* **2012**, *165*, 1−6.
(41) Wen, C.; Zhu, C.; Ju, Y.; Xu, H.; Qiu, Y. A Novel NO_2 Gas Sensor using Dual Track SAW Device. *Sens. Actuators, A* **2010**, *159*, 168−173.
(42) Blondeau-Patissier, V.; Vanotti, M.; Richard, L.; Ballandras, S. Detection and Monitoring of Hydrogen using Palladium Film on SAW. *Procedia Eng.* **2012**, *47*, 578−581.
(43) Mastromatteo, U.; Villa, F. F. High Sensitivity Acoustic Wave AlN/Si Mass Detectors Arrays for Artificial Olfactory and Biosensing Applications: A Review. *Sens. Actuators, B* **2013**, *179*, 319−327.
(44) Padma, N.; Joshi, A.; Singh, A.; Deshpande, S. K.; Aswal, D. K.; Gupta, S. K.; Yakhmi, J. V. NO_2 Sensors with Room Temperature Operation and Long Term Stability using Copper Phthalocyanine Thin Films. *Sens. Actuators, B* **2009**, *143*, 246−252.
(45) Rossignol, J.; Barochi, G.; de Fonseca, B.; Brunet, J.; Bouvet, M.; Pauly, A.; Markey, L. Development of Gas Sensors by Microwave Transduction with Phthalocyanine Film. *Procedia Eng.* **2012**, *47*, 1191−1194.
(46) Özmen, A.; Tekce, F.; Ebeoğlu, M. A.; Taşaltın, C.; Öztürk, Z. Z. Finding the Composition of Gas Mixtures by a Phthalocyanine-Coated QCM Sensor Array and an Artificial Neural Network. *Sens. Actuators, B* **2006**, *115*, 450−454.
(47) Lee, Y.-L.; Sheu, C.-Y.; Hsiao, R.-H. Gas Sensing Characteristics of Copper Phthalocyanine Films: Effects of Film Thickness and Sensing Temperature. *Sens. Actuators, B* **2004**, *99*, 281−287.
(48) Harbeck, S.; Emirik, Ö.F.; Gürol, I.; Gürek, A. G.; Öztürk, Z. Z.; Ahsen, V. Understanding the VOC Sorption Processes on Fluoro Alkyl Substituted Phthalocyanines using ATR FT-IR Spectroscopy and QCM Measurements. *Sens. Actuators, B* **2013**, *176*, 838−849.
(49) Sizun, T.; Bouvet, M.; Chen, Y.; Suisse, J.-M.; Barochi, G.; Rossignol, J. Differential Study of Substituted and Unsubstituted Cobalt Phthalocyanines for Gas Sensor Applications. *Sens. Actuators, B* **2011**, *159*, 163−170.
(50) Lee, C.; Yang, W.; Parr, R.-G. Development of the Colle-Salvetti Correlation-Energy Formula into a Functional of the Electron Density. *Phys. Rev. B* **1988**, *37*, 785.
(51) Barone, V.; Cossi, M.; Tomasi, J. A New Definition of Cavities for the Computation of Solvation Free Energies by the Polarizable Continuum Model. *J. Chem. Phys.* **1997**, *107*, 3210−3221.
(52) Frisch, M. J.; Trucks, G. W.; Schlegel, H. B.; Scuseria, G. E.; Robb, M.-A.; Cheeseman, J.-R.; Scalmani, G.; Barone, V.; Mennucci, B.; Petersson, G. A.; Nakatsuji, H.; Caricato, M.; Li, X.; Hratchian, H. P.; Izmaylov, A. F.; Bloino, J.; Zheng, G.; Sonnenberg, J. L.; Hada, M.; Ehara, M.; Toyota, K.; Fukuda, R.; Hasegawa, J.; Ishida, M.; Nakajima, T.; Honda, Y.; Kitao, O.; Nakai, H.; Vreven, T.; Montgomery, J. A., Jr.; Peralta, J-E.; Ogliaro, F.; Bearpark, M.; Heyd, J.-J.; Brothers, E.; Kudin, K.-N.; Staroverov, V.-N.; Kobayashi, R.; Normand, J.; Raghavachari, K.; Rendell, A.; Burant, J.-C.; Iyengar, S.-S.; Tomasi, J.; Cossi, M.; Rega, N.; Millam, J.-M.; Klene, M.; Knox, J.-E.; Cross, J.-B.; Bakken, V.; Adamo, C.; Jaramillo, J.; Gomperts, R.; Stratmann, R.-E.; Yazyev, O.; Austin, A. J.; Cammi, R.; Pomelli, C.; Ochterski, J.; Martin, R.-L.; Morokuma, K.; Zakrzewski, V.-G.; Voth, G.-A.; Salvador, P.; Dannenberg, J.-J.; Dapprich, S.; Daniels, A.-D.; Farkas, Ö.; Foresman, J.-B.; Ortiz, J.-V.; Cioslowski, J.; Fox, D. J. *Gassian09;* Gaussian, Inc.: Wallingford, CT, 2009.
(53) Ismat Shah, S.; Glocker. D. *Handbook of Thin Film Process Technology;* Institute of Physics Publishing: Bristol, U.K., 1995.
(54) Ensinger, W. Low Energy Ion Assist during Deposition: an Effective Tool for Controlling Thin Film Microstructure. *Nucl. Instrum. Methods Phys. Res., Sect. B* **1997**, *127*, 796−808.
(55) Tokito, S.; Sakata, J.; Taga, Y. The Molecular Orientation in Copper Phthalocyanine Thin Films Deposited on Metal film Surfaces. *Thin Solid Films* **1995**, *256*, 182−185.
(56) Petraki, F.; Peisert, H.; Biswas, I.; Chassé, T. Electronic Structure of Co-Phthalocyanine on Gold Investigated by Photoexcited Electron Spectroscopies: Indication of Co Ion-Metal Interaction. *J. Phys. Chem. C* **2010**, *114*, 17638−17643.
(57) Singh, A.; Kumar, A.; Kumar, A.; Samanta, S.; Debnath, A. K.; Jha, P.; Prasad, R.; Salmi, Z.; Nowak, S.; Chehimi, M. M.; Aswal, D. K.; Gupta, S. K. Flexible cobalt-phtalocyanine thin films with high charge carrier mobility. *Appl. Phys. Lett.* **2012**, *101* (222102), 1−5.
(58) Jackowska, K.; Krysinski, P. New Trends in the Electrochemical Sensing of Dopamine. *Anal. Bioanal. Chem.* **2013**, *405*, 3753−3771.
(59) Cabezas, C.; Pen, I.; Lopez, J.-C.; AlonsoJ, L. Seven Conformers of Neutral Dopamine Revealed in the Gas Phase. *Phys. Chem. Lett.* **2013**, *4*, 486−490.
(60) Klessinger, M.; Eckert-Maksić, M.; Maksić, Z. The Relative Stability of the Tautomers of α-Hydroxytetronic Acid. *Int. J. Quantum Chem.* **1994**, *50*, 385−394.
(61) Yadava, R. A.; Rani, P.; Kumar, M.; Singh, R.; Singh, Priyanka; Singh, N. P. Experimental IR and Raman Spectra and Quantum Chemical Studies of Molecularstructures, Conformers and Vibrational Characteristics of l-Ascorbic Acid and its anion and cation. *Spectrochim. Acta, Part A* **2011**, *84*, 6−21.
(62) Cheng, Z.; Du, S.; Guo, W.; Gao, L.; Deng, Z.; Jiang, N.; Guo, H.; Tang, T.; Gao, H.-J. Direct Imaging of Molecular Orbitals of Metal Phthalocyanines on Metal Surfaces with an O_2-functionalized Tip of a Scanning Tunneling Microscope. *Nano Res.* **2011**, *4*, 523−530.

(63) Mebs, S.; Henn, J.; Dittrich, B.; Paulmann, C.; Luger, P. Electron Densities of Three B12 Vitamins. *J. Phys. Chem. A* **2009**, *113*, 8366−8378.
(64) Dwyer, P.-N.; Madura, P.; Scheidt, R.-W. Stereochemistry of Low-Spin Cobalt Porphyrins. VI. Molecular Stereochemistry of (1,2-dimethylimidazole)-.alpha.,.beta.,.gamma.,.delta.-tetraphenyl porphinatocobalt(II). *J. Am. Chem. Soc.* **1974**, *96*, 4815−4819.
(65) Ponce, I.; Francisco Silva, J.; Onate, R.; Miranda-Rojas, S.; Munoz-Castro, A.; Arratia-Perez, R.; Mendizabal, F.; Zagal, J.-H. Theoretical and Experimental Study of Bonding and Optical Properties of Self-Assembly metallophthalocyanines Complexes on a Gold Surface. A Survey of the Substrate_Surface Interaction. *J. Phys. Chem. C* **2011**, *115*, 23512−23518.
(66) Sun, S.; Jiang, N.; Xia, D. Density Functional Theory Study of the Oxygen Reduction Reaction on Metalloporphyrins and Metallophthalocyanines. *J. Phys. Chem. C* **2011**, *115*, 9511−9517.
(67) Wäckerlin, C.; Chylarecka, D.; Kleibert, A.; Müller, K.; Iacovita, C.; Jung, T.-A.; Ballav, N. Controlling Spins in Adsorbed Molecules by a Chemical Switch. *Nat. Commun.* **2010**, *1*, DOI:10.1038/ncomms1057.